ELSEVIER SCIENCE Inc. [DTD 4.2.0]
JOURNAL AMC ARTICLE No. 6889
PAGES 1-30 DISPATCH 30 April 2001
AMC 6889
PROD. TYPE: FROM DISK
A

ELSEVIER Applied Mathematics and Computation 000 (2001) 000–000
APPLIED MATHEMATICS AND COMPUTATION
www.elsevier.com/locate/amc

Numerical solution of a complete surface energy balance model for simulation of heat fluxes and surface temperature under bare soil environment

Zhihao Qin [a,c,*], Pedro Berliner [b], Arnon Karnieli [a]

[a] *The Remote Sensing Laboratory, Department of Environmental Physics, J. Blaustein Institute for Desert Research, Ben Gurion University of the Negev, Sede Boker Campus 84990, Israel*
[b] *The Wyler Laboratory for Arid Land Conservation and Development, Department of Dryland Agriculture, J. Blaustein Institute for Desert Research, Ben Gurion University of the Negev, Sede Boker Campus 84990, Israel*
[c] *The Spatial Modelling Centre, Umeå University, P.O. Box 839, S-981 28 Kiruna, Sweden*

Abstract

Surface energy balance model is an essential approach for heat flux and evaporation estimation in applied meteorology and hydrology. Due to the complexity of soil–air interface system, the model has been simplified for different purposes in many researches. A complete model with full description of its complex factor relationships and its numerical solution has not been yet implemented in practical use. This paper presents a complete surface energy balance model with its inner relations cited from different researches. The model couples soil temperature change simultaneously with soil moisture movement, which makes the solution of the model uneasy. A detailed methodology of numerical approximation to the complete model is presented in the study for practical use. Soil heat and latent heat fluxes in the model are determined according to both soil temperature change and soil moisture movement, which are described as two differential equations. Crank–Nicolson implicit method is used to expand the differential equations into two sets of simultaneous linear equations, which are then solved by applying Gauss's elimination method. Latent heat flux is determined at the balance when evaporation from the surface is equal to the soil water loss. And surface temperature is

* Corresponding author.
E-mail addresses: zqin@ucdavis.edu, qin.zhihao@smc.kiruna.se (Z. Qin).

PII: S0096-3003(01)00089-3

estimated as the heat fluxes of the surface reaching the status of balance. The iterative computation of Newton–Raphson method is used to approximate latent heat flux and surface temperature from the balances. Based on this complexity of the model's relationships, a detailed computation procedure of the model is proposed. The methodology has been validated through application to south Israeli desert for heat flux and surface temperature estimation. By a good matching of the simulated soil temperature to the measured one proves the validity of the model and method used for its numerical solution.

Keywords: Surface energy balance model; Numerical solution; Surface temperature; Heat fluxes; Israeli desert

1. Introduction

The thought of surface energy balance has been extensively applied to various purposes especially in micro-meteorological analysis to the phenomena relating to management of the Earth's resources. Estimation of surface heat fluxes and evaporation for irrigation program is one of the most popular applications of surface energy balance theory in agriculture and forestry [5]. Actually, surface energy balance model is rather complex in terms of the involved factors and their mutual relations. Different studies used different methods to simplify the model for their specific purpose [20,25]. Generally speaking, the simplification is based on some assumptions to the parts of the model or its parameters required for the specific modeling purpose. A complete model that couples soil temperature change simultaneously with soil water movement has not been yet seen in practical use. In addition to the different focuses of different researches in the process, this probably is also due to the complex relationships involved and the difficulties of its numerical solution of the model with the complex relationships.

Different simplified models of surface energy balance have been applied for different purposes. A simple surface energy balance model is adopted by Dolman and Blyth [13] to study the behavior of the roughness length of heat and water vapor in heterogeneous terrain. Determination of evaporation is a critical part of the model. Many approaches have been proposed for the estimation of evaporation [5]. A mathematical model for the numerical computation of evaporation from bare saline soils was presented in [36]. Based on Penman–Monteith approach for evapotranspiration estimation, a land surface energy balance model is used in [14] to solve for latent and sensible heat fluxes without the need to specify a surface temperature or humidity. Ben-Asher et al. [1] assumed the surface temperature functioning as a sine curve for assessment of evaporation from bare soil. In association with remote sensing data, a surface energy balance model was used in [17] for examining the issues of land

surface properties and heat fluxes over regional scale. This model uses the known surface temperature from remote sensing data as input for heat flux estimation and does not involve the mutual determination of soil water movement and soil temperature change. In another study, Friedl [18] developed a sparse canopy model consisting of a one-dimensional, two-layer energy balance formulation based on a potential-resistance representation of the soil–canopy–atmosphere system to study the land surface fluxes from radiometric surface temperature measurements. Surface energy balance method was used in [33] to model the monthly evapotranspiration and surface energy fluxes from monthly mean satellite measurements of surface heating rate, surface temperature and normalized difference vegetation index. Blad [3] used the known surface vapor pressure to estimate energy exchange between crops and their environment. Chen and Coughour [7] developed a general model for energy and mass transfer of land surfaces by considering the soil temperature change and soil moisture movement separately. The soil temperature changes due to soil moisture movement and vice versa are neglected in the model of Chen and Coughour [7] for simplification. Using remote sensing data as inputs, Schmugge and Humes [30] applied the surface energy balance model to monitor land surface fluxes. Many studies used Bowen ratio between sensible and latent heat fluxes to estimate the evaporation rate through surface energy balance equation [5,12,20]. The existing studies using surface energy balance model do not relate soil temperature change to the simultaneous movement of soil moisture. This maybe is due to the complicated mutual relation of factors and parameters involved in the simultaneous change of soil temperature and moisture and the difficulty of computation for specific application. However, soil temperature and moisture are mutually impacted hence they are simultaneously but not separately changed in the real world. This is especially true when the soil is under a partly saturated condition. Thus, a complete model depicting this simultaneous change of soil temperature and soil moisture is required to reveal their mutual relationships and to enhance the accuracy of estimating the variation of surface heat fluxes and temperature at their equilibrium.

The objective of the paper is to present a complete surface energy balance model with its complicated inner-relationships quoted from different researches and to develop a methodology for the numerical approximation to the model. The main characteristic of the model is that it couples soil temperature change simultaneously with soil moisture movement. This simultaneous couple makes the model uneasy in computation, which probably is one of the main reasons that blocks the practical use of such a complete model. The paper intends to provide a methodology of numerical solution to the model. A detailed computation procedure of the numerical approximation is also given for practical application.

This model relates all energy parts of the soil–atmospheric system in a form as it should be in the real world and does not make any simplification for their estimation. Only a few meteorological observation data and some soil parameters are required as the inputs of the model. Through this model and its numeral solution method, it is possible to estimate surface heat fluxes, surface and soil temperature change, soil water movement and other important micro-meteorological parameters such as surface resistance change without much assumptions and simplifications to the parts of the model and its parameters. Using the meteorological data from Sede Boker in south Israeli desert, we also intend to present an example of applying the model and the methodology of its numerical solution to the south Israel desert for heat flux and surface temperature estimation.

2. The surface energy balance model

In the places where there is no heating source from the interior earth, solar radiation becomes the only source of energy controlling the most micro-meteorological events in the layer of soil–atmosphere interface. For a bare soil surface where energy storage is zero, surface energy balance at the soil–atmosphere interface can be quantitatively described as follows:

$$R_n - H - LE - G = 0, \tag{2.1}$$

where R_n is the net radiation (W m^{-2}), H is the sensible heat flux (W m^{-2}), LE is the latent heat flux (W m^{-2}), G is the soil heat flux (W m^{-2}). Because 1 W = 1 J s^{-1}, the dimension of the terms in Eq. (2.1) can also be written as J s^{-1} m^{-2} so that it is compared to the unit used in the following computation. According to the equation, net radiation R_n is equal to the sum of sensible heat into the air H, latent heat of evaporation LE and the soil heat flux G at the ground surface. The terms in Eq. (2.1) are all related to surface temperature, which becomes the key factor for numerical solution of the model.

2.1. Net radiation

The short-wave radiation from the sun reaches the top of the atmosphere at about 1395 W m^{-2}. As it passes through the atmosphere, the solar radiation is scattered, absorbed and reflected by different types of molecules and colloidal particles. Thus, the global short-wave radiation reaching the ground surface consists of the direct solar radiation and the diffuse sky radiation [5]. At the ground surface, part of the global short-wave radiation R_s is reflected by the surface into atmosphere at a density that depends on the albedo of the surface. At the same time, the Earth's surface also emits some long-wave radiation into the atmosphere and the atmosphere also emits some long-wave radiation that

reaches the ground surface. Some of the incoming atmospheric long-wave radiation is reflected by the ground surface back into the atmosphere. Therefore, at the ground surface, the net radiation can be expressed as follows after applying Stefan–Boltzmann law to the emitted terms of atmosphere and the ground

$$R_n = R_s(1-\rho) + \varepsilon_a \sigma T_a^4 \varepsilon_s \sigma T_s^4 - (1-\varepsilon_s)\varepsilon_a \sigma T_a^4, \tag{2.2}$$

where R_n is the net radiation (W m^{-2}), R_s is the global hemispheric radiation (W m^{-2}), ρ is the surface albedo, T_s is the surface temperature (K), T_a is the air temperature (K), ε_s and ε_a are the surface and air emissivities, respectively, σ is the Stefan–Boltzmann constant ($\sigma = 5.67 \times 10^{-8}$ W m^{-2} K^{-4}).

Studies indicated that air emissivity ε_a is strongly coupled to air vapor pressure (e_a) and air temperature (T_a) near the surface [5]:

$$\varepsilon_a = 1.24(e_a/T_a)^{1/7}, \tag{2.3}$$

where e_a is in mb (1 mb = 100 Pa) and T_a in K. Because air vapor pressure also has strong correlation with air temperature, ε_a also can be approximated by the empirical formula of Swinbank [32]

$$\varepsilon_a = 0.92 \times 10^{-5} T_a^2. \tag{2.4}$$

Both formula (2.3) and (2.4) have been found to yield satisfactory results with daily means at mid-latitudes and at temperature above 0°C, as well described by a standard atmosphere [5].

2.2. Sensible heat flux

Successful estimation of sensible heat flux is essential for the application of surface energy balance model [25]. Sensible heat flux H of the ground surface strongly depends on surface-air temperature difference and surface resistance to heat transfer and can be calculated by the following formula [30,35]:

$$H = \rho_a c_a (T_a - T_s)/r_a, \tag{2.5}$$

where ρ_a is the density of air ($\rho_a = 1.205$ kg m^{-3} at 20°C), c_a is the specific heat of air ($c_a = 1005$ J kg^{-1} K^{-1}), r_a is the air resistance coefficient to heat transfer (s/m), which is given as [2]

$$r_a = \frac{(\ln(z/z_0) - \varphi_h)}{kU}, \tag{2.6}$$

$$U = \frac{w_z k}{\ln(z/z_0) - \varphi_m}, \tag{2.7}$$

where u_z is the wind velocity (m s^{-1}) at standard height z ($z = 2$ m), k is Von Karman constant ($k = 0.4$), z_0 is the roughness length (m) of the surface, φ_h

and φ_m are the stability correction parameters for heat and momentum, which can be estimated through the ratio function of standard height to Monin–Obhukov length [2,9]

$$z/L_m = \frac{-kzgH}{\rho_a c_a U^3}, \tag{2.8}$$

where L_m is the Monin–Obhukov length and g the acceleration of gravity ($g = 9.8\ m/s^2$). The stability correction parameters are defined as follows [2,9]:

If $z/L_m < 0$, then

$$\varphi_h = 2\ln((1+X)/2) + \ln((1+X^2)/2) - 2\arctan(X) + \pi/2,$$
$$\varphi_m = 2\ln((1+X^2)/2).$$

If $0 < z/L_m < \ln(z/z_0)$, then $\varphi_h = \varphi_m = -5z/L_m$.

If $z/L_m \geqslant \ln(z/z_0)$, then $\varphi_h = \varphi_m = -5\ln(z/z_0)$.

Here $X = (1 - 16z/L_m)^{1/4}$ and π is the circle constant ($\pi = 3.14159265$) Therefore, the estimation of sensible heat flux requires an iterative calculation in the simulation process. The iteration could be as follows. (1) Let $\varphi_h = \varphi_m = 0$, $z/L_m = 0$ and $H1 = 0$. (2) Use Eq. (2.6) to calculate r_a. (3) Use Eq. (2.5) to calculate H. (4) Use Eq. (2.8) to calculate z/L_m. (5) Compare $H1$ and H, if $H1 - H$ is small enough to reach the required accuracy, then stop the iteration and get the final result. If not, let $H1 = H$ and compare z/L_m with $\ln(z/z_0)$ to determine the new value of φ_h and φ_m. (6) Repeat (2)–(5) until the required accuracy is reached.

2.3. Latent heat flux

The availability of energy and moisture at the earth-atmosphere interface is the critical condition for evaporation. The energy required for evaporation is generally termed as the latent heat flux LE, which can be computed by the following formula [30]:

$$LE = 0.622L(e_a - e_s)/(P_a(r_a + r_s)), \tag{2.9}$$

where e_a and e_s are the air and surface vapor pressures (kPa), respectively. P_a is the atmospheric pressure ($P_a = 101.325$ kPa). L is the latent heat of vaporization ($L = 2.543 \times 10^6\ J\ kg^{-1}$). r_s is the surface resistance ($s\ m^{-1}$), given empirically as [2]

$$r_s = 100(0.413\theta_s/\theta)^{1.5}, \tag{2.10}$$

where θ is the volumetric soil water content ($kg\ m^{-3}$) and θ_s is the volumetric soil water content at saturation ($kg\ m^{-3}$).

Actually, evaporation from ground surface must be equal to the change of soil water content in the profile. Thus, we have

$$LE - LE_c = 0, \tag{2.11}$$

where (LE_c donates the energy (W m^{-2}) caused by the change of soil water content in time interval ∂t. A complete description of soil water content change in the profile should be in three dimensions. However, in many cases, soil water movement over planar directions can be assumed to be negligibly small [5,29]. This is especially true in many arid environments where the soil water content is extremely low and the planar difference of available energy for evaporation is not significant in short distance. Under this assumption, the energy used for driving soil water movement in time interval ∂t can be computed as follows:

$$LE_c = L \int_0^z \frac{\partial \theta}{\partial t} \, dz, \tag{2.12}$$

where t is time (s) and z is the depth (m) of soil profile under consideration. $\partial\theta/\partial t$ donates the rate of soil water change. When the planar movement is neglected, the vertical movement of soil water can be described by the following differential equation [2]:

$$\begin{aligned} \partial\theta/\partial t = {} & \partial(K_c \partial\psi/\partial z)/\partial z + \partial(gK_c)/\partial z + \partial(hsD_v \partial T/\partial z)/\partial z \\ & + \partial(e_v D_v \partial h/\partial z)/\partial z, \end{aligned} \tag{2.13}$$

where K_c is the soil hydraulic conductivity (kg s m^{-3}), h is the relative humidity of the gas filled in the soil pore, ψ is the soil water potential (J $kg^{-1} = m^{-2}$ s^{-2}), s is the slope of saturated vapor pressure vs. temperature (kPa K^{-1}), e_v is the saturated vapor pressure (kPa) and D_v is the apparent vapor diffussivity (kg m^{-1} s^{-1} kPa^{-1}). Soil water potential ψ in J kg^{-1} is coupled with soil vapor pressure e in kPa and temperature T in K via equation

$$\psi = RT \ln(e/e_v) \tag{2.14}$$

in which R is the universal gas constant ($R = 461.52$ J kg^{-1} K^{-1}). Actually, soil relative humidity h is calculated as the ratio of soil vapor pressure e and saturated soil vapor pressure e_v, i.e.

$$h = e/e_v. \tag{2.15}$$

Thus, the relationship between soil water potential and relative humidity is given as $\psi = RT \ln(h)$.

The first two terms of Eq. (2.13) describe the soil water movement in liquid phase due to potential difference and gravitation, respectively. The last two terms describe the movement of soil water in the vapor phase due to temperature and potential gradients, respectively. Therefore, the change of soil water content with time is described as the function of such important variables as soil water potential, soil relative humidity and soil temperature.

2.4. Soil heat flux

Soil heat flux can be computed from soil temperature change and soil heat capacity in the profile. Usually, soil heat transfer in planar directions is negligibly small and only in vertical direction is practically worthy of consideration. Thus, the term G in (2.1) can be computed as [23]

$$G = \int_0^z C_s \frac{\partial T}{\partial t}\, dz, \tag{2.16}$$

where $\partial T/\partial t$ donates the rate of soil temperature change and C_s is the volumetric soil heat capacity (J m^{-3} K^{-1}) which can be expressed as $C_s = \rho_s c_s$, in which ρ_s is the soil density (kg m^{-3}) and c_s the specific heat of soil (J kg^{-1} K^{-1}). However, specific heat of soil is strongly dependent on soil properties especially the materials constituting the soil. It is also highly variable, depending on the change of soil water content. Usually, the soil can be viewed as constituted by soil minerals (mainly sand, silt and clay), organic materials, water and air in different proportions. Generally, the specific heat of these soil constituents is stable for practical purposes. Thus, it was suggested that heat capacity of the soil could be computed through the thermal properties of its constituents with linking to their fractions [5,26].

$$C_s = \rho_w c_w V_w + \rho_q c_q V_q + \rho_m c_m V_m + \rho_o c_o V_o + \rho_a c_a V_a, \tag{2.17}$$

where ρ is the density of soil constituents, c is the specific heat, V is the volumetric fraction, the subscripts w, q, m, o, a are referred to water, quartz, clay mineral, organic materials and air, respectively.

Natural soil is generally viewed as a poor electrical conductor [29]. This is especially true when soil water content is very low and the soil is loose or with large porosity. In this case, heat transfer in the soil by thermal conduction is ascribed to the net molecular exchange of kinetic energy, which takes place from the more energetic molecules (hotter regions) to those cooler regions where the molecular motion is less energetic [29]. In the other hand, heat transfer in the soil also causes the imbalance of energy distribution in the soil, which drives soil water movement especially in vapor form at unsaturated state. And soil water movement also eases the process of soil heat transfer. Thus, a complete description of soil heat flux must consider the equilibrium of these two factors. In the time interval ∂t, the intensity of soil heat transfer can be described by the following equation [2]:

$$C_s \partial T/\partial t = \partial(K_s \partial T/\partial z)/\partial z + \partial(hsLD_v \partial T/\partial z)/\partial z + \partial(e_v LD_v \partial h/\partial z)/\partial z, \tag{2.18}$$

where K_s is the soil thermal conductivity (W m^{-1} K^{-1}). The first term on the right-hand side of Eq. (2.18) describes the heat transfer due to temperature gradient. The second term is the energy due to soil water vapor movement under the temperature gradient. The third term is the energy due to the change

of soil water vapor distribution under the gradient of the vapor distribution in the soil.

3. Soil parameters of the model

The solution of the above surface energy balance model requires the estimation of soil parameters involved in the differential equations (2.13) and (2.18). However, most of these parameters do not have a fixed relationship with each other but depend on soil properties, especially the structure, components and textures [21]. The following empirical relationships were proposed for general purposes of estimating soil parameters required for modeling [6].

Soil thermal conductivity K_s is defined as the heat flux density conducting through the soil divided by the temperature gradient [24]. The parameter is extremely important because it strongly impacts the speed of heat transfer in the soil, which shapes soil temperature change and soil moisture movement. Like thermal capacity, thermal conductivity of natural soil is also highly variable and dependent on soil properties especially bulk density, water content, quartz content and organic matter content [6,23]. This similarity provides the similar way of computing K_s from its constituents. However, soil thermal conductivity does not have a simple relationship with the thermal conductivity of individual soil constituents because the conduction of heat takes place through all kinds of sequences of the conducting materials, in series and parallel [24]. The value of K_s depends highly on the way in which the best conducting mineral particles are interconnected by the less conducting water phases and are separated by the poorly conducting gas phase. Thus, shape factors have to be considered for the computation of K_s [2,11,36]

$$K_s = \frac{F_w V_w K_w + F_q V_q K_q + F_m V_m K_m + F_o V_o K_o + F_a V_a K_g}{F_w V_w + F_q V_q + F_m V_m + F_o V_o + F_a V_a}, \tag{3.1}$$

where V is the volumetric fraction of soil constituents, K is the thermal conductivity, F are the shape factors, and the subscripts w, q, m, o, a and g are referred to water, quartz, clay minerals, organic matters, are and gas, respectively, in the soil. The thermal conductivity of the gas which filled the soil pore K_g and the shape factors can be computed as follows:

$$\begin{aligned} &K_g = K_a + K_v, \quad K_v = 0.075e/P, \\ &F_w = V_s C_w / C, \quad F_q = V_s C_q / C, \\ &F_m = V_s C_m / C, \quad F_o = V_s C_o / C, \\ &F_a = V_a, \end{aligned}$$

where K_a is the air thermal conductivity, K_v is the apparent thermal conductivity of the gas which filled the soil pore, $K_v = 0.075e/P$, where e is the vapor

pressure and P is the total gas pressure, V_s is the volumetric fraction of soil solids ($V_s = 1 - V_a$) and C_w, C_q, C_m, C_o and C are the constants, with $C_w = 1, C_q = 0.051, C_m = 0.104, C_o = 1.298$ and $C = C_w + C_q + C_m + C_o = 2.543$.

At low water content, the air space controls the thermal conductivity of the soil and all types of soils such as litter, sand and silt loam have similar thermal conductivity. At high water content, the thermal conductivity of the solid phase becomes more important and the difference of bulk density and soil composition results in significant difference of thermal conductivity. The transition of soil thermal conductivity from low to high occurs at low water content in sand and at high water content in soils with high clay content. This relationship provides a quantitative way of computing soil thermal conductivity for modeling [6] and McInnes [27] proposed the following empirical formula for the calculation:

$$K_s = A + 2.8V_s(\theta/\rho_w)^2 + (A - B)\exp\left(-(C\theta/\rho_w)^4\right), \tag{3.2}$$

where θ is the volumetric soil water content, ρ_w is the water density ($\rho_w \approx 1000$ kg m^{-3}) and A, B and C are the parameters given as follows [6]:

$$\begin{aligned} A &= (0.57 + 1.73V_q + 0.93V_m)/(1 - 0.74V_q - 0.49V_m) - 2.8V_s(1 - V_s) \\ B &= 0.03 + 0.7V_s^2, \\ C &= 1 + 2.6/(V_c)^{1/2}, \end{aligned} \tag{3.3}$$

where V_s is the volumetric fraction of solids in soil, i.e. $V_s = V_q + V_m$.

The relationship between soil water potential and soil water content varies in different soil types [6,29]. However, the relationship does exist for specific soil. This can be expressed by the water retention curve. Campbell [6] suggested the following functional relationship between the potential and the content

$$\psi = \psi_0(\theta/\theta_s)^{-b} \tag{3.4}$$

in which ψ_0 is the soil water potential at saturation. Moreshet et al. [28] defined $\psi_0 = -4.7$ J kg^{-1} for their soil. Actually ψ_0 ranges from −9 to −0.6 J kg^{-1} and it is rational to give $\psi_0 = -5$ J kg^{-1} for many cases [6]. The parameter b is also strongly dependent on soil properties especially texture and Moreshet et al. [28] gave it as $b = 10.6$ for their soil and [2] $b = 2.5$ for his. According to Campbell [6], b can range from 24 to 2 and be estimated by the following empirical formula:

$$b = d_g^{-1/2} + 0.2\sigma_g, \tag{3.5}$$

where d_g and σ_g are the geometric mean particle diameter (mm) and geometric standard deviation, respectively, given as

$$d_g = \exp(M_c \ln D_c + M_c \ln D_c + M_c \ln D_c),$$

$$\sigma_g = \exp\left\{\left[M_c(\ln D_c - d_g)^2 + M_l(nD_l - d_g)^2 + M_d(\ln D_d - d_g)^2\right]^{1/2}\right\},$$

where D_c, D_l and D_d are the arithmetic mean diameters (mm) of clay, silt and sand, generally $D_c < 0.002$ mm, $0.002 \leqslant D_l < 0.05$ mm and $0.05 \leqslant D_d < 2.0$ mm, M_c, M_l and M_d are the mass fractions of clay, silt and sand, respectively, in the soil.

Soil hydraulic conductivity K_c has a functional relationship with the soil water content [4,26] though the determinants of the parameter are the properties of soil but not only water content. Studies indicated that different soils have different hydraulic conductivities under the same water content [5,6,26]. However, for the same soil, soil water content is the main determinant of hydraulic conductivity and the following relationship between the conductivity K_c and soil water content θ was proposed for practical calculations [4,6]:

$$K_c = K_h(\theta/\theta_s)^m, \tag{3.6}$$

where K_h is the saturated hydraulic conductivity and m is a shape parameter related to the texture of the soil [8]. Empirically, Campbell [6] gave m as $m = 2 + 3/b$ and Braud (1989) $m = 2 + 1/b$. As suggested by Campbell [6], soil saturated hydraulic conductivity K_h is calculated as

$$K_h = 0.002 \exp(-4.26(M_l + M_c)), \tag{3.7}$$

where V_s and V_c are the mass fractions of silt and clay in the soil, respectively. Generally speaking, hydraulic conductivity K_c is extremely small when soil water content is low. According to the measurement of Gardner [19], K_c of a sandy loam soil is about 5.4×10^{-12} kg s m^{-3} for $\theta = 110$ kg m^{-3} and 1.3×10^{-10} kg s m^{-3} for $\theta = 170$ kg m^{-3}. According to the graph given by Campbell [6], K_c is about 2×10^{-9} kg s m^3 for Guelph loam with water content 200 kg m^{-3} and about 2×10^{-5} kg s m^{-3} for Botany sand with water content 100 kg m^{-3}.

Apparent vapor diffusivity D_v is given by Troeh et al. [34] as

$$D_v = D_a(0.622\rho_a/P)[(V_a - u)/(1 - u)]^v \tag{3.8}$$

where P is the total gas pressure (kPa), D_a is the vapor diffussivity (m^2 s^{-1}) in the air, given by $D_a = (2.22 + 0.158T_c) \times 10^{-5}$ in which T_c is the temperature in °C, u and v are the parameters, given by Toeh et al. [34] as $u = 0.05$ and $v = 1.5$.

Saturated vapor pressure e_v is a function of the temperature given as

$$e_v = [\exp(26.6904 - 6109.74/T - 0.00916189T]/10, \tag{3.9}$$

in which T is the temperature in K. And the slope of saturated vapor pressure vs. temperature s can be calculated as

$$s = s_t e_v/(T^2), \tag{3.10}$$

where s_t is a temperature constant ($s_t = 5307$ K).

When the above soil parameters and such meteorological data as global radiation, air temperature, air relative humidity and wind speed are available, the surface energy balance model described in (2.1) can be numerically solved for estimation of heat flux and surface temperature.

4. Numerical solution to the model

Numerical solution of the model is based on the following approximations: iterative computation of latent heat flux and surface temperature, respectively, from Eqs. (2.13) and (2.1), simultaneous solution of soil temperature and soil moisture change from differential equations (2.13) and (2.18).

4.1. Newton–Raphson method for approximation

As we have seen, the relations in surface energy balance model are very complicated. It is impossible to directly express the key factor (surface temperature T_s) of the model as a function of other variables. Usually, to solve such a complicated equation our model involves the application of the numerical approximation method. Among the approximation methods, Newton–Raphson iterative technique is a good one because it can rapidly reach the solution with the required accuracy.

Because all terms of Eq. (2.1) are the functions of surface temperature (T_s), we can rewrite the equation as

$$f(T_s) = R_n - H - LE - G = 0, \tag{4.1}$$

which is a successive function within such an interval as $T_s \subseteq (-50°C, 100°C)$. Therefore, to apply Newton–Raphson iterative method for approximation, we start with the point T_s^0 in the interval $T_s^0 \subseteq (-50°C, 100°C)$ for the solution of T_s and proceed to determine additional approximation by

$$T_s^{n+1} = T_s^n - \frac{f(T_s^n)}{f'(T_s^n)} \quad (n = 0, 1, 2 \ldots), \tag{4.2}$$

where $f(T_s^n)$ and $f'(T_s^n)$ are the values of the function $f(T_s)$ and its derivative at T_s^n. Geometrically, Newton–Raphson method means that the tangent at the point $(T_s^n, f(T_s^n))$ of the curve $y = f(T_s)$ is extended to the intersection with T_s axis at T_s^{n+1}, which is used as the new approximation to the solution T_s. If T_s^n is a good approximation, it can be expected that T_s^{n+1} approximates T_s still better [16] because T_s^{n+1} is much closer to T_s. Therefore, after iterative calculation many times when $|\bar{f}(T_s^n)| \to 0$ or is less than the required accuracy, we get

$T_s^{n+1} = T_s^n \to T_s$ and stop the iterative calculation. Thus, we can conclude that T_s^n is the solution of the surface temperature T_s from the model under the balance of available inputs.

If δT is taken to be small enough, the derivative $f'(T_s^n)$ can be given as

$$f'(T_s^n) = \frac{f(T_s^n + \delta T) - f(T_s^n)}{\delta T}. \tag{4.3}$$

Thus, we have

$$T_s^{n+1} = T_s^n - \frac{f(T_s^n)\delta T}{f(T_s^n + \delta T) - f(T_s^n)}. \tag{4.4}$$

To solve the function $f(T_s)$ for T_s also involves to solve the differential equations (4.15) and (4.16) simultaneously. Crank–Nicholson technique can be used to approximate the solution of the two differential equations. This technique is mathematically complicated. A detailed description will be given in Section 5.

In order to compute the latent heat flux LE for the approximation of surface temperature T_s, Eq. (2.11) has also to be solved for vapor pressure e_s or relative humidity h_s of the ground surface. And the solution of this equation is coupled to the simultaneous solution of Eqs. (2.9) and (2.12), of which the latter has resulted from the differential equation (2.13). Due to impossibility to give a direct solution of surface humidity h_s for the computation, approximation has to be employed for the iterative calculation of h_s from Eq. (2.11). According to Eq. (2.9), the unknown for computing LE is surface vapor pressure e_s, which is related to surface relative humidity h_s through Eq. (2.16). Therefore, both LE and LE_c can be viewed as the function of h_s and we can rewrite Eq. (2.11) as

$$f(h_s) = LE - LE_c. \tag{4.5}$$

Similarly, Newton–Raphson iterative approximation method can be used to give a solution of h_s from this equation. The procedure of the solution is the same as that used for the solution of T_s from Eq. (4.1) hence not necessary to repeat.

4.2. Derivation of differential equations about soil water movement and temperature change

Using Newton–Raphson approximation to solve surface temperature and latent heat flux from Eqs. (2.1) and (2.11) involves the solution of differential equations (2.13) and (2.18). In order to solve differential equation (2.13) about soil water movement, we have to derive the equation into a proper form for approximation. According to Eqs. (2.14) and (2.15), we can rewrite the derivative $\partial\psi/\partial z$ in Eq. (2.13) as

$$\partial\psi/\partial z = \partial(RT\ln(h))/\partial z = RT\partial(\ln(h))/\partial z + R\ln(h)\partial T/\partial z$$
$$= (RT/h)\partial h/\partial z + R\ln(h)\partial T/\partial z. \quad (4.6)$$

460 Thus, the first differential term in the right-hand side of Eq. (2.13) can be re-
461 written as

$$\partial(K_c\partial\psi/\partial z)/\partial z = \partial((K_cRT/h)\partial h/\partial z + K_cR\ln(h)\partial T/\partial z)/\partial z$$
$$= \partial((RK_cT/h)\partial h/\partial z)/\partial z + \partial(RK_c\ln(h)\partial T/\partial z)/\partial z. \quad (4.7)$$

463 At the same time, the term $\partial\theta/\partial t$ can be written as

$$\partial\theta/\partial t = (\partial\theta/\partial h)\partial h/\partial t. \quad (4.8)$$

465 Let $C_h = (\partial\theta/\partial h)$, we have

$$\partial\theta/\partial t = C_h\partial h/\partial t. \quad (4.9)$$

467 The acceleration of gravity is a constant. Thus, the second terms in the right-
468 hand side of Eq. (2.13) can be simply rewritten as

$$\partial(gK_c)/\partial z = g\partial K_c/\partial z. \quad (4.10)$$

470 Therefore, Eq. (2.13) can be rewritten as

$$C_h\partial h/\partial t = \partial((RK_cT/h)\partial h/\partial z)/\partial z + \partial(RK_c\ln(h)\partial T/\partial z)/\partial z$$
$$+ g\partial K_c/\partial z + \partial(hsD_v\partial T/\partial z)/\partial z + \partial(e_vD_v\partial h/\partial z)/\partial z. \quad (4.11)$$

472 Reorganizing the right-hand side, we get

$$C_h\partial h/\partial t = \partial((RK_c\ln(h) + hsD_v)\partial T/\partial z)/\partial z$$
$$+ \partial((RK_cT/h + e_vD_v)\partial h/\partial z)/\partial z + g\partial K_c/\partial z. \quad (4.12)$$

474 For simplification, we define

$$K_a = RK_c\ln(h) + hsD_v, \quad (4.13)$$
$$K_b = RK_cT/h + e_vD_v, \quad (4.14)$$

476 where both K_a and K_b have the same dimension as J s K^{-1} m^{-3}. Substituting
477 K_a and K_b into Eq. (4.12), we get

$$C_h\partial h/\partial t = \partial(K_a\partial T/\partial z)/\partial z + \partial(K_b\partial h/\partial z)/\partial z + g\partial K_c/\partial z. \quad (4.15)$$

479 Similarly, Eq. (2.18) can be reorganized as

$$C_s\partial T/\partial t = \partial(K_d\partial T/\partial z)/\partial z + \partial(K_e\partial h/\partial z)/\partial z, \quad (4.16)$$

481 where K_d and K_e are defined as

$$K_d = K_s + hsLD_v, \quad (4.17)$$
$$K_e = e_vLD_v. \quad (4.18)$$

The dimension of K_d and K_e is J m^{-1} s^{-1}. With initial and boundary conditions, all the variables in (4.15) and (4.16) are known for time node j ($j = 0, 1, 2, 3 \ldots$) and what we need to solve from the two equations is the value of the variables for the time node $j + 1$. Therefore, initial and boundary conditions are critical for the numerical solution of the two equations.

4.3. Initial and boundary conditions

Eqs. (4.15) and (4.16) cannot be solved except the initial and the boundary conditions are given. For the time node $j + 1$, we can use the value of time node j for initial conditions. Thus, at the beginning, an initial condition is generally assumed for the solution. And after the value of $j + 1$ is computed, we use it as the initial condition for the next iteration of computation until the time we expect to stop.

There are several ways to give an initial condition at the beginning of computation. Usually it is determined according to the measurement of soil temperature and soil water content at different depths of the profile under consideration.

It is the fact that soil temperature and soil water content remain constant at specific depth from the surface during the time considered such as days. Thus, the constant value of soil temperature and water content at this depth can be used as lower boundary conditions T_n and θ_n of Eqs. (4.15) and (4.16). The upper boundary of soil temperature and soil water content for time node $j + 1$ are usually determined through a iterative computation. At the first, it is considered as a small change to the surface temperature and surface water content for time node j. Then, an iteration is performed for the given assumption of soil temperature and soil water content. Finally, the two boundary are determined as the required accuracy is reached for the solution of the model.

5. Crank–Nicholson technique for the differential equations

The difficulty of solving surface energy balance model lies on the simultaneous solution of the two differential equations (4.15) and (4.16). Theoretical solution to the differential equations is extremely difficult due to many implicit relations. Usually the differential equations can be solved through explicit approximation method but the explicit method is only valid (i.e. convergent and stable) for $\delta t/\delta z^2 \leqslant 1/2$, in which δt is the time interval between nodes j and $j + 1$, and δz the depth between soil layers i and $i + 1$ [31]. Considered the dimension of time in second and depth in meter, the explicit method will create a giant computation volume for a short period of simulation such as one day.

For example, if $\delta z = 0.1$ m, time interval has to be $\delta t \leqslant 0.005$ s in order to meet the convergent condition of the method and for simulating 1 s, it takes about 200 times of iterative computation. Crank and Nicolson [10] developed a method that reduces the total volume of calculation and is valid for all finite values of $\delta t/\delta z^2$ such as $\delta t = 60$ s and $\delta z = 0.01$ m. They approximated the differentials by the mean of its finite-difference representations on the $(j+1)$th and the jth time rows. Applying this implicit method, the differential terms of the differential equation (4.15) can be approximated as follows.

$$C_{\mathrm{h}}\partial h/\partial t = C_{hi+1/2,j}(h_{i,j+1} - h_{i,j})/\delta t, \tag{5.1}$$

$$\partial(K_{\mathrm{a}}\partial T/\partial z)/\partial z = \{K_{ai+1/2,j}[(T_{i+1,j+1}T_{i,j+1}) + (T_{i+1,j} - T_{i,j})] - K_{ai-1/2,j}[(T_{i,j+1} - T_{i-1,j+1}) + (T_{i,j} - T_{i-1,j})]\}/2\delta z^2, \tag{5.2}$$

$$\partial(K_b\partial h/\partial z)/\partial z = \{K_{bi+1/2,j}[(h_{i+1,j+1} - h_{i,j+1}) + (h_{i+1,j} - h_{i,j})] - K_{bi-1/2,j}[(h_{i,j+1} - h_{i-1,j+1}) + (h_{i,j} - h_{i-1,j})]\}/2\delta z^2, \tag{5.3}$$

$$g\partial K_{\mathrm{c}}/\partial z = g(K_{ci+1,j} - K_{ci,j})/\delta z, \tag{5.4}$$

where $C_{hi+1/2,j}, K_{ai+1/2,j}, K_{ai-1/2,j}, K_{bi+1/2,j}$ and $K_{bi-1/2,j}$ are given as:

$$C_{hi+1/2,j} = (C_{hi+1,j} + C_{hi,j})/2, \tag{5.5}$$

$$K_{ai+1/2,j} = (K_{ai+1,j} + K_{ai,j})/2, \qquad K_{bi+1/2,j} = (K_{bi+1,j} + K_{bi,j})/2, \tag{5.6}$$

$$K_{ai-1/2,j} = (K_{ai,j} + K_{ai-1,j})/2, \qquad K_{bi-1/2,j} = (K_{bi,j} + K_{bi-1,j})/2. \tag{5.7}$$

And according to Eq. (4.13), $K_{ai,j}$ and $K_{bi,j}$ are given by

$$K_{ai,j} = RK_{ci,j}\ln(h_{i,j}) + h_{i,j}s_{i,j}D_{vi,j}, \tag{5.8}$$

$$K_{bi,j} = RK_{ci,j}T_{i,j}/h_{i,j} + e_{vi,j}D_{vi,j}. \tag{5.9}$$

Thus, Eq. (4.15) can be approximated as

$$\begin{aligned} C_{hi+1/2,j}(h_{i,j+1} - h_{i,j})/\delta t &= \{K_{ai+1/2,j}[(T_{i+1,j+1} - T_{i,j+1}) + (T_{i+1,j} - T_{i,j})] \\ &\quad - K_{ai-1/2,j}[(T_{i,j+1} - T_{i-1,j+1}) + (T_{i,j} - T_{i-1,j})] \\ &\quad + K_{bi+1/2,j}[(h_{i+1,j+1} - h_{i,j+1}) + (h_{i+1,j} - h_{i,j})] \\ &\quad - K_{bi-1/2,j}[(h_{i,j+1} - h_{i-1,j+1}) + (h_{i,j} - h_{i-1,j})]\}/2\delta z^2 \\ &\quad + g(K_{ci+1,j} - K_{ci,j})/\delta z. \end{aligned} \tag{5.10}$$

Reorganization of the above equation leads to

$$
\begin{aligned}
&-K_{ai-1/2,j}T_{i-1,j+1} + (K_{ai-1/2,j} + K_{ai+1/2,j})T_{i,j+1} - K_{ai+1/2,j}T_{i+1,j+1} \\
&\quad - K_{bi-1/2,j}h_{i-1,j+1} + (K_{bi-1/2,j} + K_{bi+1/2,j} + 2Z_tC_{hi+1/2,j})h_{i,j+1} \\
&\quad - K_{bi+1/2,j}h_{i+1,j+1} \\
&\quad = 2Z_tC_{hi+1/2,j}h_{i,j} + K_{ai+1/2,j}(T_{i+1,j} - T_{i,j}) - K_{ai-1/2,j}(T_{i,j} - T_{i-1,j}) \\
&\qquad + K_{bi+1/2,j}(h_{i+1,j} - h_{i,j}) - K_{bi-1/2,j}(h_{i,j} - h_{i-1,j}) + 2\delta zg(K_{ci+1,j} - K_{ci,j}), \qquad (5.11)
\end{aligned}
$$

where $Z_t = \delta z^2/\delta t$. All terms in the right-hand side of the above equation only refer to the time interval j, which is known. Thus, we can denote the right-hand side as g_j for simplification.

$$
\begin{aligned}
g_j &= 2Z_tC_{hi+1/2,j}h_{i,j} + K_{ai+1/2,j}(T_{i+1,j} - T_{i,j}) - K_{ai-1/2,j}(T_{i,j} - T_{i-1,j}) \\
&\quad + K_{bi+1/2,j}(h_{i+1,j} - h_{i,j}) - K_{bi-1/2,j}(h_{i,j} - h_{i-1,j}) + 2\delta zg(K_{ci+1,j} - K_{ci,j}). \qquad (5.12)
\end{aligned}
$$

Thus, we have

$$
\begin{aligned}
&-K_{ai-1/2,j}T_{i-1,j+1} + (K_{ai-1/2,j} + K_{ai+1/2,j})T_{i,j+1} \\
&\quad - K_{ai+1/2,j}T_{i+1,j+1} - K_{bi-1/2,j}h_{i-1,j+1} + (K_{bi-1/2,j} + K_{bi+1/2,j} + 2Z_tC_{hi+1/2,j})h_{i,j+1} \\
&\quad - K_{bi+1/2,j}h_{i+1,j+1} = g_j. \qquad (5.13)
\end{aligned}
$$

Similarly, approximation of Eq. (4.16) leads to

$$
\begin{aligned}
&C_{si+1/2,j}(T_{i,j+1} - T_{i,j})/\delta t \\
&\quad = \{K_{di+1/2,j}[(T_{i+1,j+1} - T_{i,j+1}) + (T_{i+1,j} - T_{i,j})] \\
&\qquad - K_{di-1/2,j}[(T_{i,j+1} - T_{i-1,j+1}) + (T_{i,j} - T_{i-1,j})] \\
&\qquad + K_{ei+1/2,j}[(h_{i+1,j+1} - h_{i,j+1}) + (h_{i+1,j} - h_{i,j})] \\
&\qquad - K_{ei-1/2,j}[(h_{i,j+1} - h_{i-1,j+1}) + (h_{i,j} - h_{i-1,j})]\}/2\delta z^2. \qquad (5.14)
\end{aligned}
$$

Reorganization of the above equation results in

$$
\begin{aligned}
&-K_{di-1/2,j}T_{i-1,j+1} + (K_{di-1/2,j} + K_{di+1/2,j} + 2Z_tC_{si+1/2,j})T_{i,j+1} - K_{di+1/2,j}T_{i+1,j+1} \\
&\quad - K_{ei-1/2,j}h_{i-1,j+1} + (K_{ei-1/2,j} + K_{ei+1/2,j})h_{i,j+1} \\
&\quad - K_{ei+1/2,j}h_{i+1,j+1} = G_j, \qquad (5.15)
\end{aligned}
$$

where $G_j, K_{di+1/2,j}, K_{di-1/2,j}, K_{ei+1/2,j}$ and $K_{ei-1/2,j}$ are defined as

$$
\begin{aligned}
G_j &= 2Z_tC_{si+1/2,j}T_{i,j} + K_{di+1/2,j}(T_{i+1,j} - T_{i,j}) - K_{di-1/2,j}(T_{i,j} - T_{i-1,j}) \\
&\quad + K_{ei+1/2,j}(h_{i+1,j} - h_{i,j}) - K_{ei-1/2,j}(h_{i,j} - h_{i-1,j}), \qquad (5.16) \\
K_{di+1/2,j} &= (K_{di+1,j} + K_{di,j})/2, \qquad K_{di-1/2,j} = (K_{di,j} + K_{di-1,j})/2, \qquad (5.17) \\
K_{ei+1/2,j} &= (K_{ei+1,j} + K_{ei,j})/2, \qquad K_{ei-1/2,j} = (K_{ei,j} + K_{ei-1,j})/2. \qquad (5.18)
\end{aligned}
$$

And $K_{di,j}$ and $K_{ei,j}$ are given as

$$K_{di,j} = K_{si,j} + h_{i,j} s_{i,j} LD_{vi,j}, \tag{5.19}$$

$$K_{ei,j} = e_{vi,j} LD_{vi,j}. \tag{5.20}$$

Using Eqs. (5.13) and (5.15), we can simultaneously solve $T_{i+1,j+1}$, $T_{i,j+1}$, $T_{i-1,j+1}$, $h_{i+1,j+1}$, $h_{i,j+1}$ and $h_{i-1,j+1}$ when the initial values of these variables and boundary conditions are given. And this is our case. The details of the solution to (5.13) and (5.15) are given in the following section.

6. Gauss's method for solution of simultaneous equations

In both Eqs. (5.13) and (5.15), soil temperature T and relative humidity h for time node j are known as the initial conditions and the coefficients K_a, K_b, K_d and K_e can be computed for j. Thus, g_j and G_j are also known. For $j+1$, the upper boundary $T_{0,j+1}$ and $h_{0,j+1}$ and the bottom boundary $T_{n+1,j+1}$ and $h_{n+1,j+1}$ are also given by approximation. Therefore, the expansion of Eq. (5.13) about soil water movement in terms of relative humidity will result in the following simultaneous equations:

$$\begin{aligned}
&+ b_1 T_1 - c_1 T_2 + e_1 h_1 - f_1 h_2 = g_1,\\
&- a_2 T_1 + b_2 T_2 - c_2 T_3 - d_2 h_1 + e_2 h_2 - f_2 h_3 = g_2,\\
&\cdots\\
&- a_i T_{i-1} + b_i T_i - c_i T_{i+1} - d_i h_{i-1} + e_i h_i - f_i h_{i+1} = g_i,\\
&\cdots\\
&- a_n T_{n-1} + b_n T_n - d_n h_{n-1} + e_n h_n = g_n,
\end{aligned} \tag{6.1}$$

where T represents the soil temperature and h represent the relative humidity in soil pore for time node $j+1$. The subscript represents the soil layer. The coefficients a, b, c, d, e, f, and g in all subscripts are known. Thus, the unknowns are T and h that need to be solved.

Similarly, Eq. (5.15) about soil temperature change can also be expanded into the following simultaneous equations:

$$\begin{aligned}
&+ B_1 T_1 - C_1 T_2 + E_1 h_1 - F_1 h_2 = G_1,\\
&- A_2 T_1 + B_2 T_2 - C_2 T_3 - D_2 h_1 + E_2 h_2 - F_2 h_3 = G_2,\\
&\cdots\\
&- A_i T_{i-1} + B_i T_i - C_i T_{i+1} - D_i h_{i-1} + E_i h_i - F_i h_{i+1} = G_i,\\
&\cdots\\
&- A_n T_{n-1} + B_n T_n - D_n h_{n-1} + E_n h_n = G_n.
\end{aligned} \tag{6.2}$$

Totally, there are $2 \times n$ unknown variables and $2 \times n$ equations in (6.1) and (6.2). Thus, the unknown variables can be directly solved from the equation system by Gauss's elimination method.

To the simultaneous equations, the first equation in both (6.1) and (6.2) can be used to eliminate T_1 from the second one. Using the resulted equations from (6.1) and (6.2), h_1 can be eliminated to give a new second equation for (6.1), which is in the same form as the first one. Similarly, using the first equation in (6.1) and the second equation in (6.2) and the second equation in (6.1) and the first equation in (6.1), T_1 can be eliminated from both pair of equations. The resulted pair of equations can be used to eliminate h_1 to give another new second equation in the same form as the first one for (6.2). And the new second equation can be used to eliminate T_2 and h_2 from the third equations and so on, until finally T_{n-1} and h_{n-1} are eliminated from the last equations in (6.1) and (6.2), giving two equations with only two unknowns, T_n and h_n. These two unknowns can be easily solved from the two resulted equations. The unknowns $T_{n-1}, T_{n-2}, \ldots, T_2$ and T_1 and $h_{n-1}, h_{n-2}, \ldots, h_2$, and h_1 can then be found in turn by back-substitution.

Actually, this process can be simplified when the following substitution formula is applied for the solution of the simultaneous equations. Assume that the following stage of the elimination has been reached in (6.1) and (6.2),

$$a1_{i-1}T_{i-1} - b1_{i-1}T_i + d1_{i-1}h_{i-1} - e1_{i-1}h_i = g1_{i-1}, \tag{6.3}$$

$$-a_iT_{i-1} + b_iT_i - c_iT_{i+1} - d_ih_{i-1} + e_ih_i - f_ih_{i+1} = g_i, \tag{6.4}$$

$$A1_{i-1}T_{i-1} - B1_{i-1}T_i + D1_{i-1}h_{i-1} - E1_{i-1}h_i = G1_{i-1}, \tag{6.5}$$

$$-A_iT_{i-1} + B_iT_i - C_iT_{i+1} - D_ih_{i-1} + E_ih_i - F_ih_{i+1} = G_i, \tag{6.6}$$

where $a1_1 = b_1$, $b1_1 = c_1$, $d1_1 = e_1$, $e1_1 = f_1$ and $g1_1 = g_1$ and $A1_1 = B_1$, $B1_1 = C_1$, $D1_1 = E_1$, $E1_1 = F_1$ and $G1_1 = G_1$. Using (6.4) + (6.3) $a_i/a1_{i-1}$ to eliminate T_{i-1} leads to

$$\begin{aligned}&(b_i - b1_{i-1}a_i/a1_{i-1})T_i - c_iT_{i+1} - (d_i - d1_{i-1}a_i/a1_{i-1})h_{i-1}\\&\quad + (e_i - e1_{i-1}a_i/a1_{i-1})h_i - f_ih_{i+1}\\&\quad = g_i + g1_{i-1}a_i/a1_{i-1}.\end{aligned} \tag{6.7}$$

Similarly, eliminating T_{i-1} from (6.5) and (6.6) gives

$$\begin{aligned}&(B_i - B1_{i-1}A_i/A1_{i-1})T_i - C_iT_{i+1} - (D_i - D1_{i-1}A_i/A1_{i-1})h_{i-1}\\&\quad + (E_i - E1_{i-1}A_i/A1_{i-1})h_i - F_ih_{i+1}\\&\quad = G_i + G1_{i-1}A_i/A1_{i-1}.\end{aligned} \tag{6.8}$$

For $i = 2, 3, \ldots,$ we define

$$\begin{aligned} b1 &= b_i - b1_{i-1}a_i/a1_{i-1} \quad \text{and} \quad B1 = B_i - B1_{i-1}A_i/A1_{i-1}, \\ d1 &= d_i - d1_{i-1}a_i/a1_{i-1} \quad \text{and} \quad D1 = D_i - D1_{i-1}A_i/A1_{i-1}, \\ e1 &= e_i - e1_{i-1}a_i/a1_{i-1} \quad \text{and} \quad E1 = E_i - E1_{i-1}A_i/A1_{i-1}, \\ g1 &= g_i + g1_{i-1}a_i/a1_{i-1} \quad \text{and} \quad G1 = G_i + G1_{i-1}A_i/A1_{i-1}. \end{aligned} \tag{6.9}$$

600 And substitute into Eqs. (6.7) and (6.8), giving,

$$b1T_i - c_iT_{i+1} - d1h_{i-1} + e1h_i - f_ih_{i+1} = g1, \tag{6.10}$$

$$B1T_i - C_iT_{i+1} - D1h_{i-1} + E1h_i - F_ih_{i+1} = G1. \tag{6.11}$$

602 Similarly, using (6.6) + (6.3) $a1_i/A1_{i-1}$ to eliminate T_{i-1} leads to

$$\begin{aligned} &(b_i - B1_{i-1}a1_i/A1_{i-1})T_i - C_iT_{i+1} - (d_i - D1_{i-1}a1_i/A1_{i-1})h_{i-1} \\ &\quad + (e_i - E1_{i-1}a1_i/A1_{i-1})h_i - F_ih_{i+1} = g_i + G1_{i-1}a1_i/A1_{i-1}. \end{aligned} \tag{6.12}$$

604 Eliminating T_{i-1} from (6.4) and (6.5) gives

$$\begin{aligned} &(B_i - b1_{i-1}A_i/a1_{i-1})T_i - c_iT_{i+1} - (D_i - d1_{i-1}A_i/a1_{i-1})h_{i-1} \\ &\quad + (E_i - e1_{i-1}A_i/a1_{i-1})h_i - F_ih_{i+1} = G_i + g1_{i-1}A_i/a1_{i-1}. \end{aligned} \tag{6.13}$$

606 For $i = 2, 3, \ldots$, let

$$\begin{aligned} b2 &= b_i - B1_{i-1}a1_i/A1_{i-1} \quad \text{and} \quad B2 = B_i - b1_{i-1}A_i/a1_{i-1}, \\ d2 &= d_i - D1_{i-1}a1_i/A1_{i-1} \quad \text{and} \quad D2 = D_i - d1_{i-1}A_i/a1_{i-1}, \\ e2 &= e_i - E1_{i-1}a1_i/A1_{i-1} \quad \text{and} \quad E2 = E_i - e1_{i-1}A_i/a1_{i-1}, \\ g2 &= g_i + G1_{i-1}a1_i/A1_{i-1} \quad \text{and} \quad G2 = G_i + g1_{i-1}A_i/a1_{i-1}. \end{aligned} \tag{6.14}$$

608 And substitute into Eqs. (6.12) and (6.13), giving,

$$b2T_i - c_iT_{i+1} - d2h_{i-1} + e2h_i - f_ih_{i+1} = g2, \tag{6.15}$$

$$B2T_i - C_iT_{i+1} - D2h_{i-1} + E2h_i - F_ih_{i+1} = G2. \tag{6.16}$$

610 Using (6.10)–(6.11) $d1/D1$ to eliminate h_{i-1} leads to

$$\begin{aligned} &(b1 - B1d1/D1)T_i - (c_i - C_id1/D1)T_{i+1} + (e1 - E1d1/D1)h_i \\ &\quad - (f_i - F_id1/D1)h_{i+1} = g1 - G1d1/D1. \end{aligned} \tag{6.17}$$

612 And eliminating h_{i-1} from (6.15) and (6.16), we also get

$$\begin{aligned} &(B2 - b2D2/d2)T_i - (C_i - c_iD2/d2)T_{i+1} + (E2 - e2D2/d2)h_i \\ &\quad - (F_i - f_iD2/d2)h_{i+1} = G2 - g2D2/d2. \end{aligned} \tag{6.18}$$

614 Defining

$$
\begin{aligned}
&a1_i = b1 - B1d1/D1 \quad \text{and} \quad A1_i = B2 - b2D2/d2,\\
&b1_i = c_i - C_i d1/D1 \quad \text{and} \quad B1_i = C_i - c_i D2/d2,\\
&d1_i = e1 - E1d1/D1 \quad \text{and} \quad D1_i = E2 - e2D2/d2,\\
&e1_i = f_i - F_i d1/D1 \quad \text{and} \quad E1_i = F_i - f_i D2/d2,\\
&g1_i = g1 + G1d1/D1 \quad \text{and} \quad G1_i = G2 - g2D2/d2.
\end{aligned} \tag{6.19}
$$

616 And substituting into (6.17) and (6.18), we get

$$a1_i T_i - b1_i T_{i+1} + d1_i h_i - e1_i h_{i+1} = g1_i, \tag{6.20}$$

$$A1_i T_i - B1_i T_{i+1} + D1_i h_i - E1_i h_{i+1} = G1_i. \tag{6.21}$$

618 These two equations are exactly in the same form as those in (6.3) and (6.5).
619 Thus, they can be used for the next elimination.
620 After eliminating n times, we reach the final two pairs of equation as follows:

$$a1_n T_n + d1_n h_n = g1_n, \tag{6.22}$$

$$A1_n T_n + D1_n h_n = G1_n. \tag{6.23}$$

622 Using (6.22) $A1_n$–(6.23) $a1_n$ to eliminate T_n, we get the solution of h_n as

$$h_n = (g1_n A1_n - G1_n a1_n)/(d1_n A1_n - D1_n a1_n). \tag{6.24}$$

624 Similarly, the solution of T_n is

$$T_n = (g1_n D1_n - G1_n d1_n)/(a1_n D1_n - A1_n . d1_n) \tag{6.25}$$

626 After getting the solution of T_n and h_n, we can get all other unknowns from
627 Eqs. (6.20) and (6.21) for $i = n-1, n-2, \ldots, 1$. For convenience of derivation,
628 we define

$$g3 = g1_i + b1_i T_{i+1} + e1_i h_{i+1}, \tag{6.26}$$

$$G3 = G1_i + B1_i T_{i+1} + E1_i h_{i+1}, \tag{6.27}$$

630 in which h_{i+1} and T_{i+1} are known from (6.24) and (6.25) when $i+1 = n$, and
631 rewrite Eqs. (6.20) and (6.21) as

$$a1_i T_i + d1_i h_i = g3, \tag{6.28}$$

$$A1_i T_i + D1_i h_i = G3. \tag{6.29}$$

633 Using (6.28)$A1_i$ − (6.29)$a1_i$ to eliminate T_i, we get the solution of h_i as

$$h_i = (g3A1_i - G3a1_i)/(d1_i A1_i - D1_i a1_i). \tag{6.30}$$

635 Similarly, the solution of T_i is

$$T_i = (g3a1_i - G3A1_i)/(a1_i D1_i - A1_i d1_i). \tag{6.31}$$

637 Continuing the above procedure, we can get the solution of all unknowns.

7. Computation procedure of the model

As described above, the numerical approximation for the solution of surface energy balance model involves the re-adjustment of some given parameters in the iterative calculation. The computation actually is rather complicated. The procedure for the numerical solution of the model can be summarized as follows:

1. Read required constants and coefficients.
2. Assume initial soil temperature and water content for each layer.
3. Compute initial soil relative humidity for each layer.
4. Compute the required soil parameters: $D_v, e_{v,s}, C_h, K_c, C_s, K_s$.
5. Input data of global radiation, air temperature, air relative humidity and wind speed: R_s, T_a, h_a, u_z.
6. Give a start point of surface temperature T_s.
7. Compute net radiation R_n and sensible heat H.
8. Give a start point of surface relative humidity h_s.
9. Calculate surface vapor pressure and compute LE by Eq. (2.9).
10. Solve soil temperature T_i and relative humidity h_i from Eqs. (4.15) and (4.16) by Crank–Nicholson technique.
11. Calculate LE_c by Eq. (2.12) and compute $f(h_s)$ by Eq. (4.5).
12. If $f(h_s)$ is small enough to reach the required accuracy, then go to step (15).
13. Get a small δh and follow steps (9)–(11) to calculate $f(h_s + \delta h)$.
14. Update h_s in the form of Eq. (4.4) and repeat step (8)–(12).
15. Compute soil heat G by Eq. (2.16).
16. Compute $f(T_s)$ by Eq. (4.1).
17. If $f(T_s)$ is small enough to reach the required accuracy, then go to (20).
18. Get a small δT and follow steps (7)–(16) to calculate $f(T_s + \delta T)$.
19. Update T_s by Eq. (4.4) and repeat steps (7)–(17).
20. Output the results for the time interval: R_n, H, LE, G, T_s, h_s and so on.
21. Repeat steps (4)–(20) until the end of simulation period.

The procedure involves several iterations and the actual computation, as we can imagine, is very complicated. Using Quick BASIC 4.5, we have programmed the model for practical application. A program sketch about the computation procedure is given in Fig. 1.

8. Application of the model to south Israeli desert

In order to validate the model, we apply it to the south Israeli desert for estimation of heat fluxes and surface temperature change, using the meteorological data from Sede Boker Meteorological Observation Station. The Station locates in the center of an alluvial plain with about 2 km width stretching from east to west. In the north of the plain are the low hills with about 20 m high

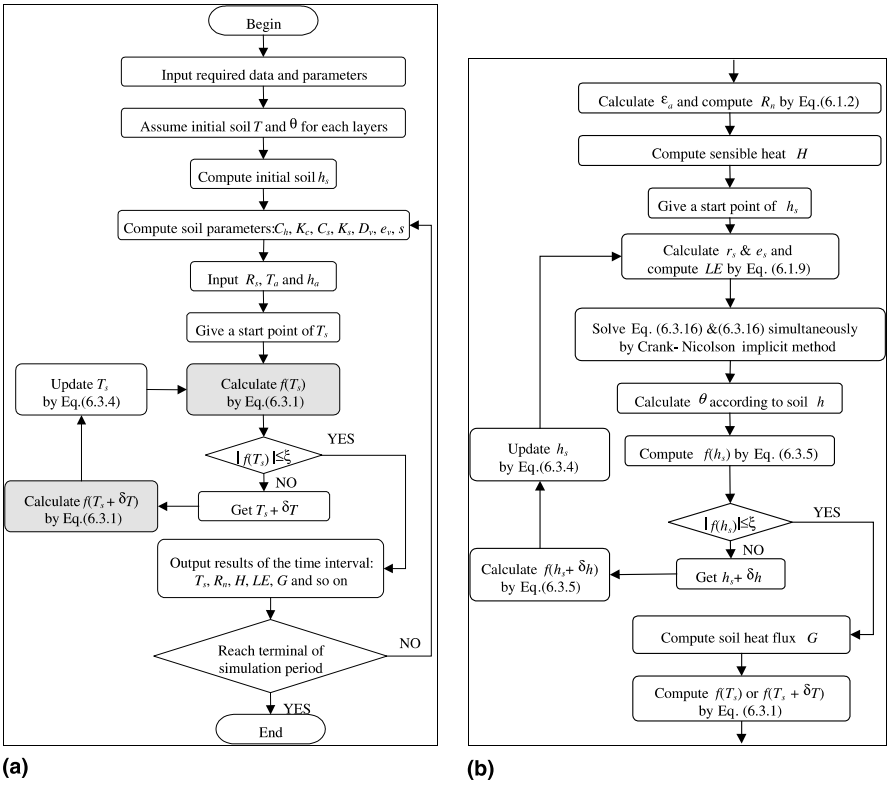

Fig. 1. (a) The main flow chart of the model. (b) The flow chart of the shaded boxes. ξ is the required accuracy for the computation.

above the plain and in the south is a long crater with about 50 m depth and 1 km width. The data of 16 July 1998 are selected for the validation of the model. It was the hot dry season of the region and the dynamics of micro-meteorological events was subjected to local conditions. The sky of July 16 was very clear and it represented the general case of the season. The soil is gray alluvium mainly composed of silt and clay. Albedo of the soil is about 30% and volumetric soil water content ranges from about 85 kg m^{-3} at the surface to 120 kg m^{-3} at 50 cm depth.

The required inputs of meteorological data include global radiation, air temperature and relative humidity and wind speed. As shown in Fig. 2(a), global radiation R_s on 16 July changed smoothly according to the angle of the sun and maximum was about 1000 W m^{-2} in the hour 12:00–13:00. Air temperature T_a had a little bit fluctuation especially in the hours 3:00–6:00. Maximal T_a was about 35°C and minimal T_a about 20°C (Fig. 2(c)). Air relative

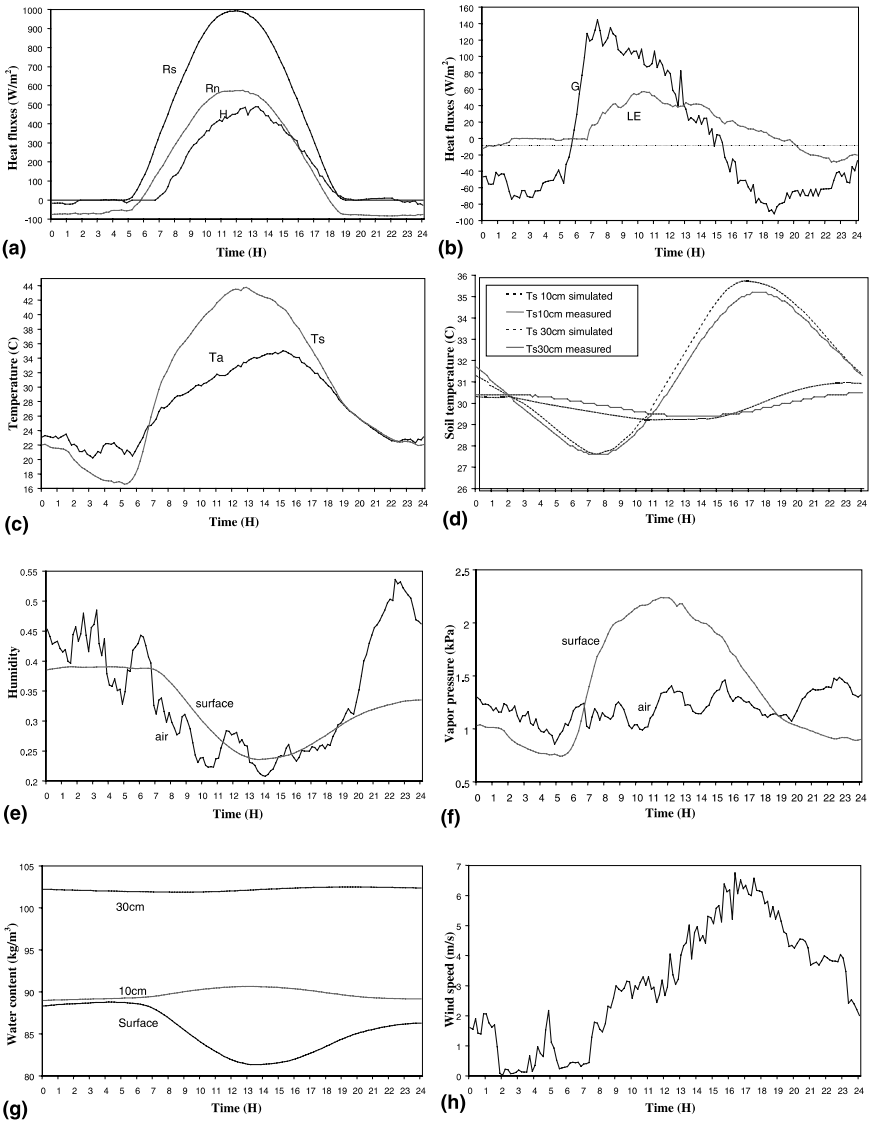

Fig. 2. Validation of the model through application to south Israeli desert, illustrating some results of the simulation and the inputs of meteorological data: (a) global radiation, net radiation and sensible heat flux; (b) soil and latent heat fluxes; (c) surface and air temperature; (d) comparison of soil temperature; (e) surface and air relative humidity; (f) surface and air vapor pressure; (g) soil water content; (h) wind speed.

humidity fluctuated from 20% to 30% during the day to 35–53% during the night (Fig. 2(e)). High variability was the common feature of wind speed (Fig. 2(h)). Maximal wind speed appeared in late afternoon due to the temperature gradient across the plain from hills to the crater.

Comparison of the simulated to the measured soil temperature at 10 cm and 30 cm depths is shown in Fig. 2(d). The measured soil temperature shown in Fig. 2(d) is a typical one in south Israeli desert. Similar change was found in [15,37]. The very close change of simulated soil temperature to the measured one proves the high validity of the model. The average difference of simulated and measured soil temperature is within 0.4°C with maximum of 0.95°C at 10 cm depth and within 0.3°C with maximum of 0.53°C at 30 cm. The ratio of the difference to the daily vibration of soil temperature is usually used to evaluate the accuracy of simulation. In our case, the daily vibration of soil temperature was about 7°C at 10 cm depth. Thus, the ratio is about 5.71%, which is quite small, hence indicates a quite accurate simulation.

According to the simulation, the daily change of heat fluxes in the arid alluvial plain is estimated as shown in Figs. 2(a) and (b). Maximal net radiation is about 575 W m^{-2} at noon and most of the net radiation is dissipated as sensible heat flux H into the air. Maximal H is about 485 W m^{-2}, accounting for above 84% of the net radiation. Maximal soil heat flux G does not appear at noon but in early morning at about 7:00–8:00 when air and surface temperatures increase rapidly. At noon soil heat flux is only about 50 W m^{-2}, accounting for about 9% of net radiation. From about 15:00 soil heat becomes negative and this means that soil releases its absorbed heat into the air for energy balance. Latent heat flux LE reaches peak in late morning at around 10:00. From about 19:00 LE becomes negative, which means that there are some moistures released as dew from the air into the soil. Integration of LE indicates that total net evaporation of the region is about 0.404 kg/m^2 or 0.404 mm per day, with evaporation into the air 0.562 mm and moisture absorption from the air 0.158 mm per day. And this is the general case of the arid region and is in accordance with the result of Ben-Asher et al. [1], who found that the evaporation from bare soil in arid environment is about 0.5 mm per day.

The estimation of land surface temperature T_s change is shown in Fig. 2(c). This change of T_s is quite reasonable in the region. During the day, the surface is very hot but it is very cool during the night. Maximal T_s occurs at about 12:00, which is about 2.5 h earlier than the peak of T_a. Minimal T_s is found to be at about 5:00 when T_a is also very low. The difference of T_s and T_a is high up to 10°C at noon while at midnight T_s is only about 1°C lower than T_a. More importance is that the land surface temperatures computed from satellite image observed at midnight and noon of the day are very close to the simulation result. Based on the remote sensing data of NOAA-AVHRR 14 with a pixel size of 1.1 × 1.1 km, T_s around Sede Boker is estimated to be about 20–23°C at

midnight (about 0:35) and 40–42°C at 14:15. This closeness of satellite observation to simulated T_s further confirms the validation of the model.

The simulation result of soil water change is just the same as the expected one (Fig. 2(g)). Soil water content θ on the surface fluctuates within the range 80–90 kg m^{-3}. Because of net evaporation, surface θ tends to decrease gradually. Evaporation during the day makes the surface very dry (about 81.4 kg m^{-3}). However, the absorption of moisture from the air lets the surface become wet (about 88.8 kg m^{-3}) during the night. Due to very low hydraulic conductivity ($< 10^{-10}$ kg s m^{-3}), θ has a little change at 10 cm and remains quite stable at 30 cm (Fig. 2(g)).

Fig. 2(e) shows the change of the simulated surface relative humidity h_s and the measured air relative humidity h_a and Fig. 3(f) shows the corresponding change of surface vapor pressure e_s and air vapor pressure e_a. The combinated functioning of evaporation and high temperature makes h_s very low during the day. The opposite functioning of the two forces drives h_s increasing. According to Eq. (2.9), evaporation occurs when the surface has higher vapor pressure than the air. Otherwise, some moisture will be released as dew from the air when e_s is lower than e_a. This process can be clearly shown in Fig. 2(f).

Other parameters such as surface resistance coefficient to heat transfer and to evaporation can also be simulated through application of the model. Considering the volume limit of the paper, we do not present the simulation results of these parameters.

We also apply the model to the data set of 1997 in the same season for mutual validation. The simulated soil temperature of the model at 10 cm depth also has a good matching with the measured one (Fig. 3(a)). Due to difference in air temperature and air humidity, the accuracy of soil temperature matching for the data set is with an average difference of about 0.6°C with maximum of

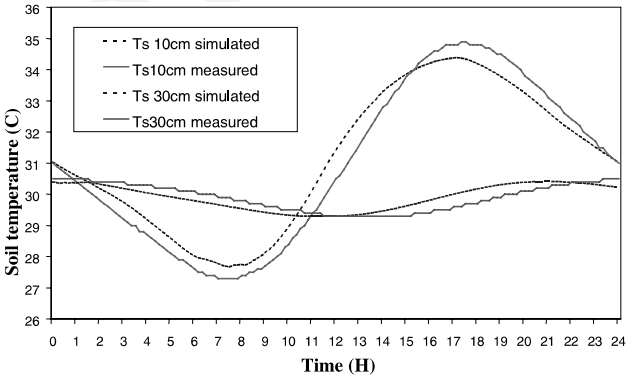

Fig. 3. Validation of the model for another data set (5 July 1997) illustrating the comparison of the simulated and the measured soil temperatures at various depths.

1.2°C at 10 cm depth. The daily vibration of soil temperature was about 8°C. Thus, the ratio of the difference to the daily vibration is about 7.5%, which is also quite small. Therefore, we can conclude that the simulation results are very close to what actually happen in the arid alluvial plain.

The successfulness of applying the model to estimate heat fluxes and surface temperature for micro-meteorological analysis lies in the successful determination of required soil parameters. It is very important to reasonably determine the parameters in Eqs. (3.1) or (3.2), (3.3) and (3.4) for computing soil water potential, hydraulic conductivity and thermal conductivity and the roughness for computing surface resistance to heat transfer. Besides, a proper way of performing the simulation procedure is also very important for numerical solution of the model. In the above simulation, we employ 1 min for time interval. For the soil profile, we consider 0.5 m depth because daily soil heat penetration in the region is limited within this depth. The thickness of soil layer is arranged to be 2 cm so that totally we have 25 layers. Time interval greater than 5 min and soil layer thicker than 10 cm may not be very good for an accurate simulation. And usually it is better to run the model for 2–3 days before the simulation results for the destination day are outputted.

9. Conclusion

A complete description of surface energy balance model is given in the current paper. The model couples soil temperature change with soil moisture movement for estimation of soil heat flux and latent heat flux. Through the two essential factors, i.e. surface temperature and surface moisture change, the model can be numerically solved for various study purposes such as irrigation program and micro-meteorological analysis. The numerical solution of the model involves the estimation of the dynamics of heat fluxes and many useful soil–water and meteorological parameters required for earth resource management.

A methodology of numerical solution to the model is presented with details so that it can be easily programmed for application of the model to the real world. Soil and latent heat fluxes are determined by soil temperature change and soil moisture movement, which can be described as differential equations. Crank–Nicolson implicit method is used to expand the differential equations into two sets of simultaneous linear equations, which are then solved by applying Gauss's elimination method. The successful application of the two critical techniques is the basis for the numerical solution of the model.

The change of soil moisture within a time interval is equal to the evaporation from the ground surface within the interval. Newton–Raphson approximation method is used for the iterative computation of solving latent heat flux to meet this requirement. This approximation method is also applied to the solution of

surface temperature from the model. Because the method is rather complicated, a detailed computation procedure for numerical solution of the model is also presented. Using this procedure, heat fluxes and temperature change can be easily estimated from the model when the required soil parameters and meteorological data are available. And this is the general case. Therefore, the methodology presented herein provides an easy way of applying surface energy model to simulate the dynamics of many micro-meteorological phenomena in the soil–air interface.

Using the meteorological data from Sede Boker in south Israeli desert, an example has been given to illustrate the application of the model and its numerical solution for heat flux and surface temperature estimation. Good matching of the simulated soil temperature to the measured one proves the validity of the model and its numerical solution method. At about noon, net radiation accounts for about 60% of the incident global radiation. Sensible heat flux is the main dissipation of the net radiation due to very low evaporation and soil heat flux. Above 85% of net radiation is dissipated as sensible heat into the air. Total net evaporation in the arid region is about 0.404 mm per day, with actual evaporation of 0.562 mm from the surface during the day and moisture absorption 0.158 mm from the air during the night. Surface temperature is high up to about 43.7°C at noon. The surface temperature peak is 2.5 hours ahead of air temperature. Therefore, at noon the maximal surface and air temperature difference is up to 10.4°C. The ground is cooler than the air during the night but the difference is much smaller than that during the day. The land surface temperature around Sede Boker on remote sensing data of NOAA-AVHRR 14 is also very close to the simulated surface temperature at noon and midnight. This closeness further confirms the validity of the model and its numerical solution. However, the successfulness of applying the model to the real world relies on the successful determination of soil parameters especially those for soil water potential, soil hydraulic and thermal conductivity as well as a proper way of running the model.

10. Uncited reference

[22]

Acknowledgements

The authors would like to thank the International Center for Desert Research, J. Blaustein Institute for Desert Research, Ben Gurion University of the Negev for offering a fellowship to Qin Zhihao to conduct the research. We also

would like to extend our thanks to the Laboratory of Desert Meteorology, Dept. of Environmental Physics J. Blaustein Institute for Desert Research, Ben Gurion University of the Negev for providing the required meteorological data used in the study.

References

[1] J. Ben-Asher, A.D. Mathhias, A.W. Warrick, Assessment of evaporation from bare soil by infrared thermometry, Soil Sci. Soc. Am. J. 47 (1983) 185–191.
[2] P.R. Berliner, Contribution of heat dissipated at the soil surface to the energy balance of a citrus orchard, Ph.D. Thesis, Hebrew University, Jerusalem, Israel, 1988.
[3] B.L. Blad, Energy exchange among leaf, canopy and environment, in: I.D. Teare, M.M. Peat (Eds.), Crop–Water Relations, Wiley, New York, USA, 1983, pp. 1–39.
[4] I. Braud, Spatial variability of surface properties and estimation of surface fluxes of a savannah, Agric. Forestry Meteorol. 89 (1998) 15–44.
[5] W. Brutsaert, Evaporation into the Atmosphere: Theory, History and Application, D. Reidel Publishing Company, Dordrecht, Holland, 1982.
[6] G.S. Campbell, Soil Physics with Basic: Transport Models for Soil–Plant Systems, Elsevier, Amsterdam, The Netherlands, 1985.
[7] D.X. Chen, M.B. Coughenour, GEMTM: a general model for energy and mass transfer of land surfaces and its application at the FIFE sites, Agric. Forestry Meteorol. 68 (1994) 145–171.
[8] B.J. Choudhury, C.A. Federer, Some sensitivity results for corn canopy temperature and its spatial variation included by soil hydraulic heterogeneity, Agric. Forestry Meteorol. 31 (1984) 297–317.
[9] D. Courault, J.P. Lagouarde, B. Aloui, Evaporation for maritime catchment combining a meteorological model with vegetation information and airborne surface temperatures, Agric. Forestry Meteorol. 82 (1996) 93–117.
[10] J. Crank, P. Nicolson, A practical method for numerical evaluation of solutions of partial differential equations of the heat conduction types, Proc. Cambridge Philos. Soc. 43 (1947) 50–67.
[11] D.A. De Vries, Thermal properties of soils, in: W.R. Van Wijk (Ed.), Physics of Plant Environment, North-Holland, Amsterdam, The Netherlands, 1963, pp. 210–235.
[12] G.R. Diak, M.S. Whipple, Improvements to models and methods for evaluating the land surface energy balance and 'effective' roughness using radiosonde reports and satellite-measured 'skin' temperature data, Agric. Forestry Meteorol. 63 (1993) 189–218.
[13] A.J. Dolman, E.M. Blyth, Patch scale aggregation of heterogeneous land surface cover for mesoscale meteorological models, J. Hydrol. 190 (1997) 252–268.
[14] A.J. Dolman, A multi-source land surface energy balance model for use in general circulation models, Agric. Forestry Meteorol. 65 (1993) 21–45.
[15] C. Fania, G. Zipora, Soil Temperature Regime in Israel, Israel Meteorogical Service, Bet Dagon, Israel, 1997.
[16] H. Flanders, J.J. Price, Calculus with Analytic Geometry, Academic Press, New York, USA, 1978.
[17] M.A. Friedl, Relationships among remotely sensed data, surface energy balance, and area-averaged fluxes over partially vegetated land surfaces, J. Appl. Meteorol. 35 (1996) 2091–2103.
[18] M.A. Friedl, Modeling land surface fluxes using a sparse canopy model and radiometric surface temperature measurements, J. Geophys. Res. 100 (1995) 25435–25446.

[19] W.R. Gardner, Calculation of capillary conductivity from pressure plate outflow data, Proc. Soil Sci. Soc. Am. 20 (1956) 317–320.
[20] M.V. Gutiérrez, F.C. Meinzer, Energy balance and latent heat flux partitioning in coffee hedgerows at different stages of canopy development, Agric. Forestry Meteorol. 68 (1994) 173–186.
[21] R.J. Hanks, G.L. Ashcroft, Applied Soil Physics: Soil Water and Temperature Applications, Springer, New York, USA, 1980.
[22] M.A. Hares, M.D. Novak, Simulation of surface energy balance and soil temperature under strip tillage: I Model description, Soil Sci. Soc. Am. J. 56 (1992) 22–29.
[23] B.A. Kimball, R.D. Jackson, Soil heat flux, in: B.J. Barfield, J.F. Gerber (Eds.), Modification of the Aerial Environment of Plants, American Society of Agricultural Engineers, St. Joseph, MI, USA, 1979, pp. 211–229.
[24] P. Koorevaar, G. Menelik, C. Dirksen, Elements of Soil Physics, Elsevier, Amsterdam, Holand, 1983.
[25] J.P. Lhomme, B. Monteny, M. Amadou, Estimating sensible heat flux from radiometric temperature over sparse millet, Agric. Forestry Meteorol. 68 (1994) 77–91.
[26] T.J. Marshall, J.W. Holmes, Soil Physics, Cambridge University Press, Cambridge, UK, 1979.
[27] K.J. McInnes, Thermal conductivity of soils from dryland wheat regions of Eastern Washington, M.S. Thesis, Washington State University, Pullman, USA, 1981.
[28] S. Moreshet, I. Cohen, M. Fuchs, Response of mature "Shamouti" orange trees to irrigation of different soil volumes at similar levels of available water, Irrigation Sci. 3 (1983) 223–236.
[29] C.W. Rose, Agricultural Physics, Pergamon Press, Oxford, Britain, 1969.
[30] T. Schmugge, K. Humes, ASTER observations for the monitoring of land surface fluxes, J. Jap. Remote Sensing Soc. 15 (1995) 83–89.
[31] G.D. Smith, Numerical Solution of Partial Differential Equations: Finite Difference Methods, Oxford University Press, Oxford, Britain, 1978.
[32] W.C. Swinbank, Long-wave radiation from clear shies, Quart. J. Roy. Meteorol. Soc. 8 (1963) 339–348.
[33] J.D. Tarpley, Monthly evapotranspiration from satellite and conventional meteorological observations, J. Climate 7 (1994) 704–713.
[34] F.R. Troeh, J.D. Jabro, D. Kirkham, Gaseous diffusion equations for porous materials, Geoderma 27 (1982) 239–253.
[35] S.B. Verma, B.J. Barfield, Aerial and crop resistance affecting energy transport, in: B.J. Barfield, J.F. Gerber (Eds.), Modification of the Aerial Environment of Plants, American Society of Agricultural Engineers, St. Joseph, MI, USA, 1979, pp. 230–248.
[36] A. Yakirevich, P. Berliner, S. Sorek, A model for numerical simulating of evaporation from bare saline soil, Water Resour. Res. 33 (1997) 1021–1033.
[37] Z. Zemel, J. Lomas, Soil Temperature Regime in Israel as a Basis for Agricultural Planning, Israel Meteorogical Service, Bet Dagon, Israel, 1977.